Computational Methods for Differential Equations
http://cmde.tabrizu.ac.ir
Vol. 6, No. 2, 2018, pp. 215-237

The smoothed particle hydrodynamics method for solving generalized variable coefficient Schrödinger equation and Schrödinger-Boussinesq system

Gholamreza Karamali
Faculty of Bsic Sciences, Shahid Sattari Aeronautical University of Siences and Technology, South Mehrabad, Tehran, Iran.
E-mail: gh_karamali@azad.ac.ir

Mostafa Abbaszadeh*
Faculty of Bsic Sciences, Shahid Sattari Aeronautical University of Siences and Technology, South Mehrabad, Tehran, Iran.
E-mail: m.abbaszadeh@aut.ac.ir

Mehdi Dehghan
Department of Applied Mathematics, Faculty of Mathematics and Computer Sciences, Amirkabir University of Technology, No. 424, Hafez Ave., 15914, Tehran, Iran.
E-mail: mdehghan@aut.ac.ir, mdehghan.aut@gmail.com

Abstract A meshless numerical technique is proposed for solving the generalized variable coefficient Schrödinger equation and Schrödinger-Boussinesq system with electromagnetic fields. The employed meshless technique is based on a generalized smoothed particle hydrodynamics (SPH) approach. The spatial direction has been discretized with the generalized SPH technique. Thus, we obtain a system of ordinary differential equations (ODEs). Also, in the numerical methods for solving the time-dependent PDEs, based on the meshless methods, to achieve acceptable results, the temporal direction must be discretized using an effective technique. Thus, in the current paper, we apply the fourth-order exponential time differenceing Runge-Kutta method (ETDRK4) for the obtained system of ODEs. The aim of this paper is to show that the meshless method based on the generalized SPH approach is suitable for the treatment of the nonlinear complex partial differential equations. Numerical examples confirm the efficiency of proposed scheme.

Keywords. Nonlinear generalized variable coefficient Schrödinger equation, Electromagnetic fields, Schrödinger-Boussinesq system, Meshless method, Smoothed particle hydrodynamics method, Fourth-order exponential time differenceing Runge-Kutta method.

2010 Mathematics Subject Classification. 65M70, 34A34.

1. Introduction

Natural phenomena can be described by partial differential equations (PDEs). Nonlinear phenomena play important role in applied mathematics, physics and also in engineering problems in which each parameter varies depending on different factors. As said in [34], many phenomena in engineering and applied sciences are modeled by

Received: 28 July 2017 ; Accepted: 6 March 2018.
∗ Corresponding author.

nonlinear evolution equations [34]. Solitonary solutions of nonlinear evolution equations provide better understanding of the physical mechanism of phenomena [34]. The knowledge of closed form solutions of nonlinear partial differential equations facilitates the testing of numerical solvers, aids in the stability analysis of solutions and conduces to a better understanding of nonlinear phenomena that these equations model [13]. Also, the search of exact solution for nonlinear partial differential equations is very difficult. Therefore, numerical methods are useful for solving nonlinear partial differential equations.

In this paper, we consider two models that one of them is the generalized Schrödinger equation with variable coefficients

$$\begin{aligned} & i\frac{\partial u}{\partial t} + a(t)\frac{\partial^2 u}{\partial x^2} + b(t)\frac{\partial^2 u}{\partial y^2} + c(t)\frac{\partial^2 u}{\partial z^2} + h(t)f(|u|^2)u + v(x,y)u = 0, \\ & (x,y,z,t) \in \Omega \times (0,T], \end{aligned} \tag{1.1}$$

with Dirichlet boundary condition

$$u(x,y,z,t) = g(x,y,z,), \qquad (x,y,z,t) \in \partial\Omega, \tag{1.2}$$

and initial condition

$$u(x,y,z,0) = k(x,y,z), \qquad (x,y,z) \in \Omega. \tag{1.3}$$

List of the works have been done on this problem includes: a linearized finite-difference scheme [4], a compact split-step finite difference method [8], a spatial sixth-order alternating direction implicit method [23], a compact finite difference scheme [24], fourth-order compact and energy conservative difference schemes [42], meshless collocation method based on the radial basis functions [7], four alternating direction implicit (ADI) schemes [52], split-step orthogonal spline collocation (OSC) methods [41], the tanh method and the sine–cosine method [43, 44], etc.

The other one is also the Schrödinger-Boussinesq system

$$\begin{cases} i\dfrac{\partial u}{\partial t} + \gamma\Delta u = \xi uv, & \mathbf{x} \in \mathbb{R}^d, \quad t > 0, \\ \dfrac{\partial^2 v}{\partial t^2} = \Delta v - \alpha\Delta^2 v + \Delta(f(v)) + \omega\Delta(|u|^2), & \mathbf{x} \in \mathbb{R}^d, \quad t > 0, \end{cases} \tag{1.4}$$

in which the complex function u and the real function v denote the electric field of Langmuir oscillations and the low-frequency density perturbation, respectively.

Problem (1.4) has been solved by many numerical techniques for example a continuum limit for a diatomic lattice system with a cubic nonlinearity [53], the existence and uniqueness of the global solutions with initial value problem or periodic boundary value problem [14], the global existence of solutions and the long time behavior of nonlinear Schrodinger-Boussinesq equations with zero order dissipation

[16], the local and global well-posedness of the periodic boundary value problem for the nonlinear Schrodinger-Boussinesq system [11], existence of solution for dissipative Schrodinger-Boussinesq equations [25], the attractor and its regularity of the damped Schrodinger-Boussinesq equation [15], complex coupled Higgs field equation and coupled Schrodinger-Boussinesq equation [18], G/G'-expansion method is used to construct exact periodic and soliton solutions of nonlinear Schrodinger-Boussinesq system [21], the new exact traveling wave solutions of the coupled Schrodinger-Boussinesq equation by using the extended simplest equation method [3], analytical solutions of a generic system of coupled ordinary differential equations for a pair of real scalar fields [36], five important and general solitary wave solutions for Schrodinger-Boussinesq equation [38], combination of boundary knot method and meshless analog equation method [9], time-splitting method combined with with the Chebyshev pseudo-spectral [40], Kansa's approach, RBFs-Pseudo-spectral (PS) method and generalized moving least squares (GMLS) method [10], time-splitting combined with exponential wave integrator Fourier pseudospectral method [28], the time-splitting Fourier spectral method [1], a multi-symplectic Hamiltonian formulation [22], a Not-a-Knot meshless method using radial basis functions and predictor-corrector scheme [39], a conservative difference scheme [55], two conserved compact finite difference schemes [27], a quadratic B-spline finite-element method [2], etc.

2. Smoothed Particle Hydrodynamics (SPH) method

One of the local meshless methods is smoothed particle hydrodynamics (SPH) that is presented in [12, 33]. The SPH technique is a computational method used for simulating the dynamics of continuum media, such as solid mechanics and fluid flows. The SPH method is a mesh-free Lagrangian method where the coordinates move with the fluid, and the resolution of the method can easily be adjusted with respect to variables such as the density. The SPH method is based on dividing the fluid into a set of discrete elements that they are well-known as "particles". These particles have a spatial distance over which their properties are "smoothed" by a kernel function. This means that the physical quantity of any particle can be obtained by summing the relevant properties of all the particles which lie within the range of the kernel. Also, the SPH method is employed for the shallow water equation. The interested readers can find more information on SPH method in [45]

Wei and et. al. [46] applied the SPH method to investigate the impact of a tsunami bore on simplified bridge piers in this study. This work was motivated by observations of bridge damage during several recent tsunami events. The main aim of [47, 48] is to apply the numerical model of GPUSPH, an implementation of the weakly compressible Smoothed Particle Hydrodynamics method on graphics processing units, to investigate tsunami forces on bridge superstructures and tsunami mitigation on bridges by using a service road bridge and an offshore breakwater. Authors of [49] investigated vorticity generation by short-crested wave breaking by using the mesh-free Smoothed Particle Hydrodynamics model.

The SPH is a computational method used for simulating the dynamics of continuum media, such as cell-wise strain smoothing operations into conventional finite elements and the smoothed finite element method (SFEM) for 2D elastic problems

[30]. The SPH technique has been studied by many researchers such as a corrected parallel SPH (C-SPH) method to simulate the 3D generalized Newtonian free surface flows with low Reynolds' number [37], distributed memory parallelization of particle methods [35], a novel caching algorithm for Computing Unified Device Architecture (CUDA) shared memory [50], an improved weakly compressible SPH method to simulate transient free surface flows of viscous and viscoelastic fluids [51], a low-dissipation weakly-compressible SPH method for modeling free-surface flows exhibiting violent events [54], etc. Also, the interested readers can find more details for SPH method in [31, 32],

In this section, we describe the meshless smoothed particle hydrodynamics meshless method. The main idea for this method is based on the integral representation of a field function $u(x)$ as follows

$$\langle u(\mathbf{x})\rangle = \int_{\Omega} u(\mathbf{x}')W(\mathbf{x}-\mathbf{x}',h)d\mathbf{x}', \tag{2.1}$$

in which

(1) W is smoothing function or kernel function,
(2) h is the smoothing length defining the influence area of W.

The integral representation (2.1) is convergent when W satisfies the following conditions:

$$\int_{\Omega} W(\mathbf{x}-\mathbf{x}',h)d\mathbf{x}' = 1, \tag{2.2}$$

$$\lim_{h\to 0} W(\mathbf{x}-\mathbf{x}',h) = \delta(\mathbf{x}-\mathbf{x}'), \tag{2.3}$$

$$W(\mathbf{x}-\mathbf{x}',h) > 0, \qquad \text{on } \Omega, \tag{2.4}$$

$$W(\mathbf{x}-\mathbf{x}',h) = 0, \qquad when \quad |\mathbf{x}-\mathbf{x}'| > kh, \tag{2.5}$$

in which k is a constant which is a measure of the effective (non-zero) area of the smoothing function centered at a point having position vector $\mathbf{x}$. The mentioned effective area is well-known as the support domain. Based on the condition (2.5), the integration over the computational domain can be reduced over the support domain thus we have a localized technique. Let the smoothing function W be an even function in $\mathbf{x}$. Then using the Taylor series expansion of function $u(\mathbf{x})$ around $\mathbf{x}$ and the condition (2.2), it can be seen that the representation of $u(\mathbf{x})$ has the second-order $O(h^2)$ accuracy. Also, it must be mentioned that this is true for interior regions and for the boundary regions, we can not obtain the second-order accuracy.

By discretizing the continuous integral representation (2.1), we can get the particle approximation as follows:

$$\langle u(\mathbf{x})\rangle \simeq \sum_j \frac{m_j}{\rho_j} u_j W(\mathbf{x}-\mathbf{x}_j, h), \tag{2.6}$$

in which m_j and ρ_j are the mass and density of the particle j, respectively. In other hand, $\frac{m_j}{\rho_j}$ gives the volume V_j respected to j. The particle approximation for the spatial derivative $\frac{\partial u(\mathbf{x})}{\partial \mathbf{x}}$ can be obtained by substituting function $u(\mathbf{x})$ with $\frac{\partial u(\mathbf{x})}{\partial \mathbf{x}}$ in relation (2.1). Using the integration by parts and also employing the divergence theorem, we can get

$$\left\langle \frac{\partial u(\mathbf{x})}{\partial \mathbf{x}} \right\rangle = \int_{\partial\Omega} u(\mathbf{x}')W(\mathbf{x}-\mathbf{x}_j, h)\mathbf{n}ds - \int_{\Omega} u(\mathbf{x}')\frac{\partial W(\mathbf{x}-\mathbf{x}', h)}{\partial \mathbf{x}'}d\mathbf{x}'. \tag{2.7}$$

The first boundary integral term has been eliminated. Thus, Eq. (2.7) can be written as follows:

$$\left\langle \frac{\partial u(\mathbf{x})}{\partial \mathbf{x}} \right\rangle \simeq -\sum_j \frac{m_j}{\rho_j} u_j \frac{\partial W(\mathbf{x}-\mathbf{x}_j, h)}{\partial \mathbf{x}_j}. \tag{2.8}$$

Finally, the particle approximation for a function and its derivatives at particle i can be written to the following form:

$$u_i = \sum_j \frac{m_j}{\rho_j} u_j W_{ij}, \tag{2.9}$$

$$\left(\frac{\partial u(\mathbf{x})}{\partial \mathbf{x}}\right)_i = \sum_j \frac{m_j}{\rho_j}\left(u_j - u_i\right)\frac{\partial W_{ij}}{\partial \mathbf{x}_i}, \tag{2.10}$$

in which

$$W_{ij} = W(\mathbf{x}_i - \mathbf{x}_j, h), \qquad \frac{\partial W_{ij}}{\partial \mathbf{x}_i} = \frac{\partial W(\mathbf{x}_i - \mathbf{x}_j, h)}{\partial \mathbf{x}_i}.$$

The smooth function is an important issue in the SPH method that it has direct effect on accuracy, efficiency and stability of the resulting algorithm. There are several selections to the smooth function such as Gaussian functions, spline functions, etc. In the current paper, we have used the quintic spline function to the following form

$$W_{ij} = W(r,h) = \lambda_0 \times \begin{cases} (3-\lambda)^5 - 6(2-\lambda)^3 + 15(1-\lambda)^5, & 0 \le \lambda < 1, \\ (3-\lambda)^5 - 6(2-\lambda)^3, & 1 \le \lambda < 2, \\ (3-\lambda)^5, & 2 \le \lambda < 3, \\ 0, & \lambda \ge 3, \end{cases} \tag{2.11}$$

in which

$$r = \left\|\mathbf{x}_i - \mathbf{x}_j\right\|, \qquad \lambda = \frac{r}{h}, \qquad \lambda_0 = \frac{7}{478\pi h^2}. \tag{2.12}$$

3. A generalized SPH method

In the current section, we employ the developed approach in [5] and also, this section is taken from [5]. Using the Taylor series for u about the point (x_i, y_i), multiplying both sides with a kernel function W and integrating over the entire domain Ω yield [5]

$$\begin{aligned}
&\int_\Omega u(\hat{x})W dx = u(\hat{x}_i)\int_\Omega W dx + u_x(\hat{x}_i)\int_\Omega (x-x_i)W dx \\
&+u_y(\hat{x}_i)\int_\Omega (y-y_i)W dx + \frac{u_{xx}(\hat{x}_i)}{2}\int_\Omega (x-x_i)^2 W dx \\
&+u_{xy}(\hat{x}_i)\int_\Omega (x-x_i)(y-y_i)W dx + \frac{u_{yy}(\hat{x}_i)}{2}\int_\Omega (y-y_i)^2 W dx + \dots
\end{aligned} \tag{3.1}$$

thus a corrective version of the kernel and particle approximations may be obtained as [5]

$$u(\widehat{x}_i) = \frac{\int_\Omega u(\widehat{x})W dx}{\int_\Omega W dx}, \tag{3.2}$$

and [5]

$$u_i = \frac{\sum_{j=1}^{N} \frac{m_j}{\rho_j} W_{ij} u_j}{\sum_{j=1}^{N} \frac{m_j}{\rho_j} W_{ij}}. \tag{3.3}$$

So, the derivative approximations in 1D case are [5]

$$u_{xi} \approx \frac{\int_\Omega [u(x)-u_i]\,\widehat{W} dx}{\int_\Omega (x-x_i)\widehat{W} dx}, \tag{3.4}$$

$$u_{xxi} \approx \frac{\int_\Omega [u(x)-u_i]\,\widehat{W} dx - u_{xi}\int_\Omega (x-x_i)\widehat{W} dx}{\frac{1}{2}\int_\Omega (x-x_i)^2 \widehat{W} dx}. \tag{3.5}$$

But in the two-dimensional case, there is not a straightforward way similar to 1D case. Ignoring the second-order derivatives and also higher terms in Eq. (3.1), for the two first derivatives f_{xi} and f_{yi} gives [5]

$$f_{x_i}\int\limits_{\Omega}(x-x_i)W_{,x}dx+f_{y_i}\int\limits_{\Omega}(y-y_i)W_{,x}dx = \int\limits_{\Omega}(f-f_i)W_{,x}dx, \tag{3.6}$$

$$f_{x_i}\int\limits_{\Omega}(x-x_i)W_{,y}dx+f_{y_i}\int\limits_{\Omega}(y-y_i)W_{,y}dx = \int\limits_{\Omega}(f-f_i)W_{,y}dx. \tag{3.7}$$

Replacing kernel function W by the anti-symmetric functions $W_{,x}$ and $W_{,y}$ in relations (3.6) and (3.7), the particle approximations may be obtained as

$$\mathbf{A}_{\alpha\beta i}\mathbf{u}_{\beta i}=\mathbf{F}_{\alpha i}, \tag{3.8}$$

in which [5]

$$\mathbf{A}_{\alpha\beta i}=\sum_{j=1}^{N}(\beta_j-\beta_i)\frac{m_j}{\rho_j}W_{ij,\alpha}, \qquad \mathbf{F}_{\alpha\beta i}=\sum_{j=1}^{N}(f_j-f_i)\frac{m_j}{\rho_j}W_{ij,\alpha}, \tag{3.9}$$

where α and β represent the spatial coordinates x and y, respectively, and also $W_{ij,\alpha}=\dfrac{\partial W(\overline{x}_j-\overline{x}_i;h)}{\partial\alpha_j}$. Finally, by solving the system of equations (3.8), we can obtain the two first-order derivatives at particle i. Also to approximate the three second-order derivatives, the following system must be solved

$$\begin{bmatrix} A_{xxxxi} & A_{xxxyi} & A_{xxyyi} \\ A_{xyxxi} & A_{xyxyi} & A_{xyyyi} \\ A_{yyxxi} & A_{yyxyi} & A_{yyyyi} \end{bmatrix}\begin{bmatrix} u_{xxi} \\ u_{xyi} \\ u_{yyi} \end{bmatrix}=\begin{bmatrix} G_{xxi}-A_{xxxi}u_{xi}-A_{xxyi}u_{yi} \\ G_{xyi}-A_{xyxi}u_{xi}-A_{xyy}u_{yi} \\ G_{yyi}-A_{yyxi}u_{xi}-A_{yyyi}u_{yi} \end{bmatrix}, \tag{3.10}$$

in which [5]

$$A_{\xi\eta\alpha\beta i} = \sum_{j=1}^{N}(\alpha_j-\alpha_i)(\beta_j-\beta_i)\frac{m_j}{\rho_j}W_{ij,\xi\eta}, \tag{3.11}$$

$$A_{\xi\eta\alpha i} = \sum_{j=1}^{N}(\alpha_j-\alpha_i)\frac{m_j}{\rho_j}W_{ij,\xi\eta}, \tag{3.12}$$

$$G_{\xi\eta i} = \sum_{j=1}^{N}(f_j-f_i)\frac{m_j}{\rho_j}W_{ij,\xi\eta}. \tag{3.13}$$

4. GSPH discretization for Schrödinger and Schrödinger-Boussinesq models

In the current section, we describe implementing the GSPH technique on the two considered models.

At first, we consider the first model i.e. the generalized Schrödinger equation with variable coefficients as follows

$$i\frac{\partial u}{\partial t}+a(t)\frac{\partial^2 u}{\partial x^2}+b(t)\frac{\partial^2 u}{\partial y^2}+h(t)f(|u|^2)u+v(x,y)u=0, \qquad (x,y,z,t)\in\Omega\times(0,T]. \tag{4.1}$$

Eq. (4.1) at particle k can be rewritten as

$$i\frac{\partial u_k}{\partial t}+a(t)\frac{\partial^2 u_k}{\partial x^2}+b(t)\frac{\partial^2 u_k}{\partial y^2}+h(t)f(|u_k|^2)u_k+v(x_k,y_k)u_k=0. \tag{4.2}$$

By substituting relations (3.3) and (3.11)-(3.13) in Eq. (4.2), we can obtain a system of ODEs. Also, for the Schrödinger-Boussinesq system

$$\begin{cases} i\dfrac{\partial u}{\partial t}+\gamma\Delta u=\xi uv, & \mathbf{x}\in\mathbb{R}^d, \quad t>0,\\[2mm] \dfrac{\partial^2 v}{\partial t^2}=\Delta v-\alpha\Delta^2 v+\Delta(f(v))+\omega\Delta(|u|^2), & \mathbf{x}\in\mathbb{R}^d, \quad t>0, \end{cases} \tag{4.3}$$

using the relations

$$w=v_t, \qquad \Delta v=z, \tag{4.4}$$

Eq. (4.3) can be rewritten as follows

$$\begin{cases} i\dfrac{\partial u}{\partial t}+\gamma\Delta u=\xi uv, & \mathbf{x}\in\mathbb{R}^d, \quad t>0,\\[2mm] \dfrac{\partial w}{\partial t}=z-\alpha\Delta z+\Delta(f(v))+\omega\Delta(|u|^2), & \mathbf{x}\in\mathbb{R}^d, \quad t>0,\\[2mm] \dfrac{\partial v_k}{\partial t}=w_k, & \mathbf{x}\in\mathbb{R}^d, \quad t>0,\\[2mm] z=\Delta v, & \mathbf{x}\in\mathbb{R}^d, \quad t>0. \end{cases} \tag{4.5}$$

Similar to previous model, Eq. (4.5) at particle k can be rewritten as

$$\begin{cases} i\dfrac{\partial u_k}{\partial t}+\gamma\Delta u_k=\xi u_k v_k, & \mathbf{x}\in\mathbb{R}^d, \quad t>0,\\[2mm] \dfrac{\partial w_k}{\partial t}=z_k-\alpha\Delta z_k+\Delta(f(v_k))+\omega\Delta(|u_k|^2), & \mathbf{x}\in\mathbb{R}^d, \quad t>0,\\[2mm] \dfrac{\partial v_k}{\partial t}=w_k, & \mathbf{x}\in\mathbb{R}^d, \quad t>0,\\[2mm] z_k=\Delta v_k, & \mathbf{x}\in\mathbb{R}^d, \quad t>0, \end{cases}$$

(4.6)

Eqs. (4.2) and (4.6) are system of ODEs that must be solved using a numerical approach with acceptable and effective numerical technique. In the current paper, we use the fourth-order exponential time differenceing Runge-Kutta method (ETDRK4) to solve the obtained system of ODEs [6, 19, 20, 26]. The ETDRK4 method can be used for discritizing the following ordinary differential equation

$$U_t + AU = F(U,t). \tag{4.7}$$

Liang et. al. [26] proposed an improved ETDRK4 method which we can bypass the inversion of the complex stiffness matrix. The improved ETDRK4 method can be split as follows [26]

Step 1.: $\left(\tau A - \widetilde{d_1} I\right)\alpha = \widetilde{\omega_1} U_h^n + \tau \widetilde{\zeta_1} F\left(U_h^n, t_n\right),$
Step 2.: $a^n = U_h^n + 2\Re(\alpha),$
Step 3.: $\left(\tau A - \widetilde{d_1} I\right)\beta = \widetilde{\omega_1} U_h^n + \tau \widetilde{\zeta_1} F\left(a^n, t_n + \frac{\tau}{2}\right),$
Step 4.: $b^n = U_h^n + 2\Re(\beta),$
Step 5.: $\left(\tau A - \widetilde{d_1} I\right)\gamma = \widetilde{\omega_1} a^n + \tau \widetilde{\zeta_1}\left[2F\left(b^n, t_n + \frac{\tau}{2}\right) - F\left(U_h^n, t_n\right)\right],$
Step 6.: $b^n = a^n + 2\Re(\gamma),$
Step 7.: $(\tau A - d_1 I)\,\phi = \omega_1 u_h^n + \tau\omega_{11} F\left(U_h^n, t_n\right) + \tau\omega_{21}\left[F\left(a^n, t_n + \frac{\tau}{2}\right) + F\left(b^n, t_n + \frac{\tau}{2}\right)\right] + \tau\omega_{31} F\left(c^n, t_n + \tau\right),$
Step 8.: $U_h^{n+1} = U_h^n + 2R(\phi).$

In the above, $\Re(z)$ denotes the real part of z and the appeared coefficients are as follows [26]

$$\begin{aligned}
d_1 &= -3.0 + i1.73205080756887729352,\\
\omega_1 &= -6.0 - i10.3923048454132637611,\\
\omega_{11} &= -0.5 - i1.44337567297406441127,\\
\omega_{21} &= -i1.15470053837925152901,\\
\omega_{31} &= 0.5 + i0.28867513459481288225,\\
\widetilde{d_1} &= -6.0 + i3.4641016151377545870548,\\
\widetilde{\omega}_1 &= -12.0 - i20.78460969082652752232935,\\
\zeta_1 &= -i3.46410161513775458705.
\end{aligned}$$

5. Numerical simulations

In this part we tabulate the numerical results of procedure applied on six test problems. We test the accuracy with the stability of new numerical formula described here by performing the described algorithm for different values of h and τ. We performed our computations using **Matlab** 7 software on a Pentium IV, 2800 MHz CPU machine with 4 Gbyte of memory.

5.1. **Test problem 1.** We consider the one-dimensional Schrodinger equation to the following form [8]

$$i\frac{\partial u}{\partial t} + \alpha\frac{\partial^2 u}{\partial x^2} + 2|u|^2 u = 0, \tag{5.1}$$

FIGURE 1. Approximation solution with absolute error at different values of final time for Test problem 1.

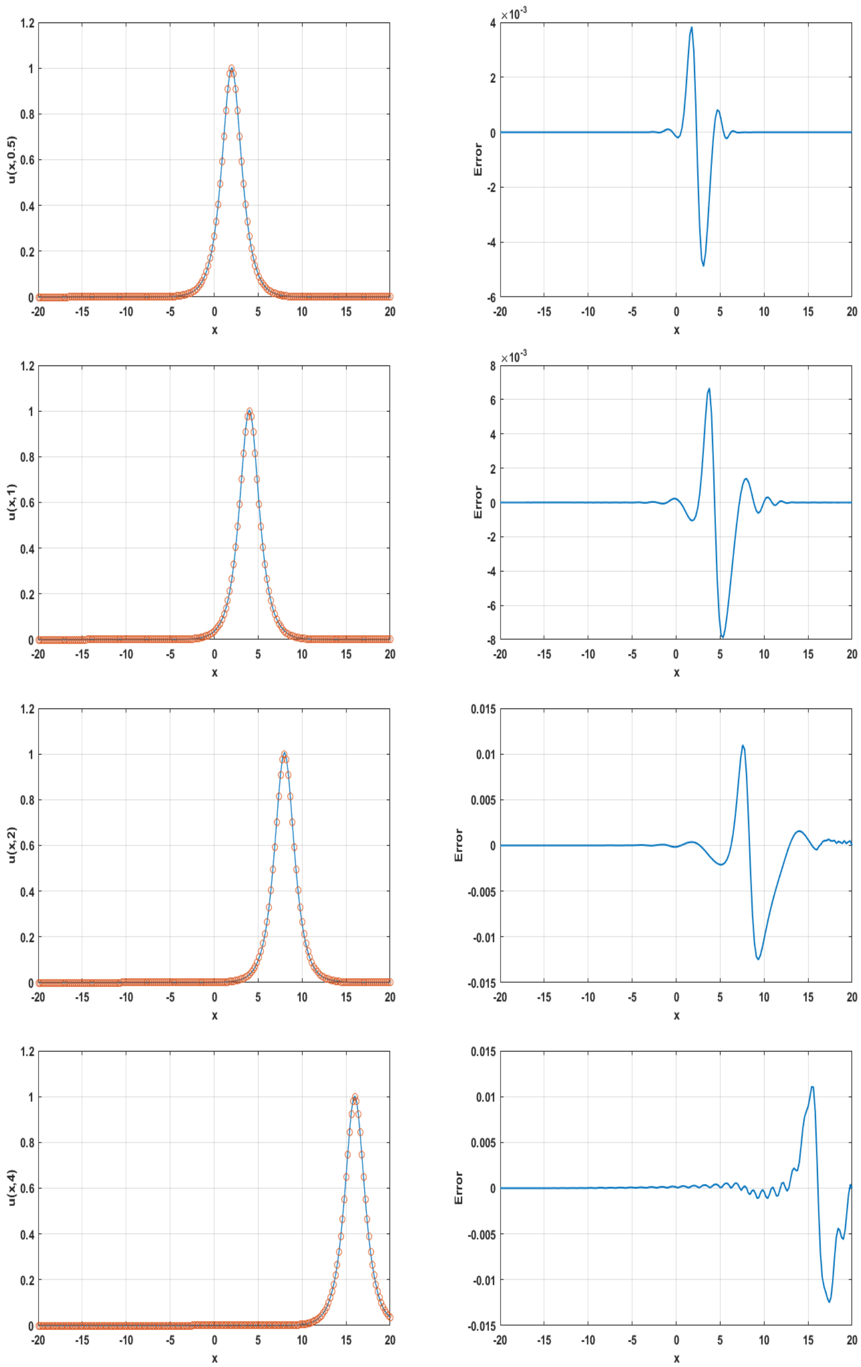

with the exact solution

$$u(x,t) = \exp(i(2x - 3t))\,\mathrm{sech}(x - 4t). \tag{5.2}$$

Table 1. Error obtained at final time $T = 1$ for Test problem 1

h	$\Omega = [-1,1]$	$\Omega = [-2,2]$	$\Omega = [-4,4]$	$\Omega = [-6,6]$
1/10	4.8075×10^{-3}	1.6398×10^{-1}	8.9726×10^{-1}	9.0734×10^{-1}
1/15	5.8183×10^{-4}	2.0774×10^{-2}	5.4933×10^{-1}	5.7749×10^{-1}
1/20	1.1278×10^{-4}	3.7477×10^{-3}	1.4802×10^{-1}	4.5039×10^{-1}
1/25	4.1711×10^{-5}	8.9945×10^{-4}	7.0163×10^{-2}	3.6619×10^{-1}
1/30	2.0383×10^{-5}	3.0698×10^{-4}	3.1438×10^{-2}	9.0734×10^{-1}
1/35	1.2480×10^{-5}	1.0706×10^{-4}	1.4774×10^{-2}	5.7749×10^{-2}
1/40	6.2955×10^{-6}	4.3497×10^{-5}	7.5061×10^{-3}	4.5039×10^{-2}
1/45	4.9113×10^{-6}	2.5921×10^{-5}	4.0960×10^{-3}	3.6619×10^{-2}
1/50	4.8947×10^{-6}	2.1068×10^{-5}	2.5885×10^{-3}	3.6619×10^{-2}

We solve the current problem using the explained technique. Table 1 shows the error obtained at final time $T = 1$ for Test problem 1. Also, Table 2 shows the error obtained at final time $T = 1$ for Test problem 1. In other word, from Tables 1 and 2, we can see the convergence of the proposed method at final time $T = 1$ on the different computational domains. Figure 1 presents the graphs of approximation solution with absolute error on computational domain $\Omega = [-20, 20]$ and at different values of final time for Test problem 1. Table 3 shows a comparison between obtained errors of the developed technique in [8] with $h = 0.1$ and $k = 0.01$ and the method presented in this paper with $\tau = 10^{-3}$ and $h = 0.01$ for Test problem 1.

5.2. **Test problem 2.** In the current problem, we consider the generalized Schrodinger equation with variable coefficients as follows [17]

$$i\frac{\partial u}{\partial t} + a(t)\frac{\partial^2 u}{\partial x^2} + b(t)\frac{\partial^2 u}{\partial y^2} + h(t)f(|u|^2)u + v(x,y)u = 0, \tag{5.3}$$

Table 2. Error obtained at final time $T = 2$ for Test problem 1

h	$\Omega = [-1,1]$	$\Omega = [-2,2]$	$\Omega = [-3,3]$	$\Omega = [-4,4]$
1/10	4.4881×10^{-3}	2.2697×10^{-1}	8.5223×10^{-1}	5.0966×10^{-1}
1/15	2.6023×10^{-3}	2.2651×10^{-1}	5.0009×10^{-1}	2.3033×10^{-1}
1/20	1.5122×10^{-4}	4.4425×10^{-3}	1.9165×10^{-2}	4.0682×10^{-1}
1/25	4.3466×10^{-5}	8.4246×10^{-4}	6.4934×10^{-3}	9.7671×10^{-2}
1/30	2.0333×10^{-5}	3.1114×10^{-4}	2.6018×10^{-3}	3.4509×10^{-2}
1/35	1.2489×10^{-5}	2.0784×10^{-4}	1.1426×10^{-3}	1.5225×10^{-2}
1/40	8.7301×10^{-6}	8.7946×10^{-5}	5.0972×10^{-4}	7.7305×10^{-3}

TABLE 3. Comparison between obtained errors for component u Test problem 1

T	Compact SSFD-ADI [8]		Present Method,	
	L_∞	L_2	L_∞	L_2
0.5	1.939×10^{-3}	2.845×10^{-3}	9.210×10^{-3}	7.591×10^{-3}
1	3.721×10^{-3}	5.672×10^{-3}	7.989×10^{-3}	6.989×10^{-3}
2	7.848×10^{-3}	1.237×10^{-2}	4.041×10^{-2}	1.501×10^{-2}
3	1.242×10^{-2}	1.969×10^{-2}	2.653×10^{-2}	1.010×10^{-2}
4	3.674×10^{-2}	3.662×10^{-2}	4.210×10^{-2}	3.983×10^{-2}

FIGURE 2. Approximation solution with its contour and graph of absolute error at final time $T = 1$ for Test problem 3.

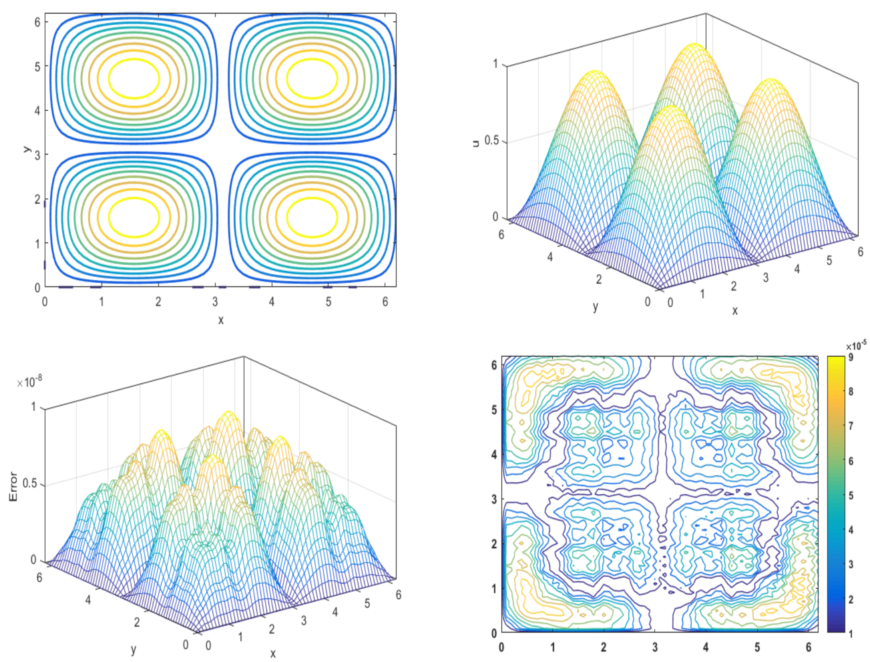

with

$$a(t) = b(t) = \frac{1}{2}, \quad h(t) = 1, \quad f(|u|^2) = -|u|^2, \quad v(x, y) = -(1 - \sin^2(x)\sin^2(y)), \tag{5.4}$$

then the exact solution will be

$$u(x,y,t) = \exp(-2it)\sin(x)\sin(y). \tag{5.5}$$

Table 4. Error obtained at different final time for Test problem 2

h	$T=1$	$T=2$	$T=5$	$T=10$
$\pi/20$	5.4458×10^{-8}	7.3915×10^{-8}	1.5154×10^{-7}	9.0734×10^{-7}
$\pi/40$	1.1524×10^{-8}	4.4714×10^{-8}	8.1866×10^{-8}	5.7749×10^{-7}
$\pi/50$	8.8191×10^{-9}	1.0471×10^{-8}	3.5151×10^{-8}	4.5039×10^{-8}
$\pi/60$	5.0042×10^{-9}	9.1124×10^{-9}	1.0931×10^{-8}	3.6619×10^{-8}

Table 5. Comparison between obtained errors for component u Test problem 2

	Linearized CCD-ADI [17]		Present Method	
h	L_∞	L_2	L_∞	L_2
$\pi/4$	7.41×10^{-4}	3.50×10^{-4}	6.38×10^{-3}	4.85×10^{-3}
$\pi/8$	1.56×10^{-5}	5.86×10^{-6}	8.29×10^{-5}	2.93×10^{-5}
$\pi/16$	2.00×10^{-7}	8.87×10^{-8}	1.48×10^{-5}	4.39×10^{-6}

We solve this problem using the proposed technique. Table 4 presents the error obtained at different values of final time for Test problem 2. Figure 2 illustrates the graphs of approximation solution with its contour and absolute error at final time $T=1$ for Test problem 2.

5.3. **Test problem 3.** We consider the one-dimensional Schrodinger equation to the following form [8]

$$i\frac{\partial u}{\partial t} + \alpha\Delta u + 2|u|^2 u = 0, \qquad (x,y)\in\Omega, \tag{5.6}$$

with the exact solution

$$u(x,t) = \exp(i(2x+2y-3t))\,\mathrm{sech}(x+y-4t). \tag{5.7}$$

We obtain the approximation solution for the current problem based on the proposed technique. Table 6 demonstrates the error obtained on computational domain $\Omega = [-5,5]\times[-5,5]$ and at different values of final time for Test problem 3. Figure 3 displays the contour of approximation solution at different values of final times for Test problem 3.

TABLE 6. Error obtained on computational domain $\Omega = [-5,5] \times [-5,5]$ for Test problem 3

n_s	$T = 0.5$	$T = 1$	$T = 2$	$T = 4$
5	4.9271×10^{-2}	9.6457×10^{-2}	4.0655×10^{-1}	8.4320×10^{-1}
10	1.9591×10^{-2}	3.7942×10^{-2}	1.1741×10^{-1}	3.5578×10^{-1}
20	2.1420×10^{-3}	4.7193×10^{-3}	1.5396×10^{-2}	7.8103×10^{-2}
30	8.2119×10^{-4}	1.7754×10^{-3}	1.9787×10^{-3}	5.3219×10^{-3}
40	2.4108×10^{-4}	7.0226×10^{-4}	8.4317×10^{-4}	1.0412×10^{-3}

5.4. **Test problem 4.** We consider the Schrödinger-Boussinesq system as [28]

$$\begin{cases} i\dfrac{\partial u}{\partial t} + \gamma u_{xx} = \xi u v, & x \in \Omega, \quad t > 0, \\ \dfrac{\partial^2 v}{\partial t^2} = v_{xx} - \alpha v_{xxxx} + (f(v))_{xx} + \omega(|u|^2)_{xx}, & x \in \Omega, \quad t > 0, \end{cases} \tag{5.8}$$

with exact solution

$$\begin{cases} u(x,t) = \pm\dfrac{6b_1}{\xi}\sqrt{\dfrac{\gamma\theta - \alpha\xi}{\gamma\omega}}\,\mathrm{sech}(\mu\zeta)\tanh(\mu\zeta)e^{i\left(\frac{M}{2\gamma}+\delta t\right)}, \\ v(x,t) = -\dfrac{6b_1}{\xi}\sec h^2(\mu\zeta), \end{cases} \tag{5.9}$$

in which

$$b_1 = \delta + \frac{M^2}{4\gamma}, \qquad d_1 = 1 - M^2, \qquad \mu = \sqrt{\frac{b_1}{\gamma}},$$

$$\zeta = x - Mt, \qquad \gamma = 1, \qquad \xi = 1, \qquad \alpha = 1,$$

$$\theta = \frac{4}{3}, \qquad \omega = \frac{1}{18}, \qquad M = \frac{1}{\sqrt{5}}, \qquad \delta = \frac{1}{12}.$$

We solve this equation using the proposed technique. Table 7 presents the error obtained to show the accuracy and computational order of time-discrete scheme with $h = 1/300$ for Test problem 4.

Table 8 demonstrates a comparison between errors obtained based on the developed techniques in [28, 29] with $\tau = 10^{-4}$ and the present method with $\tau = 10^{-5}$ for Test problem 4.

FIGURE 3. Contour of approximation solution at different values of final times for Test problem 3.

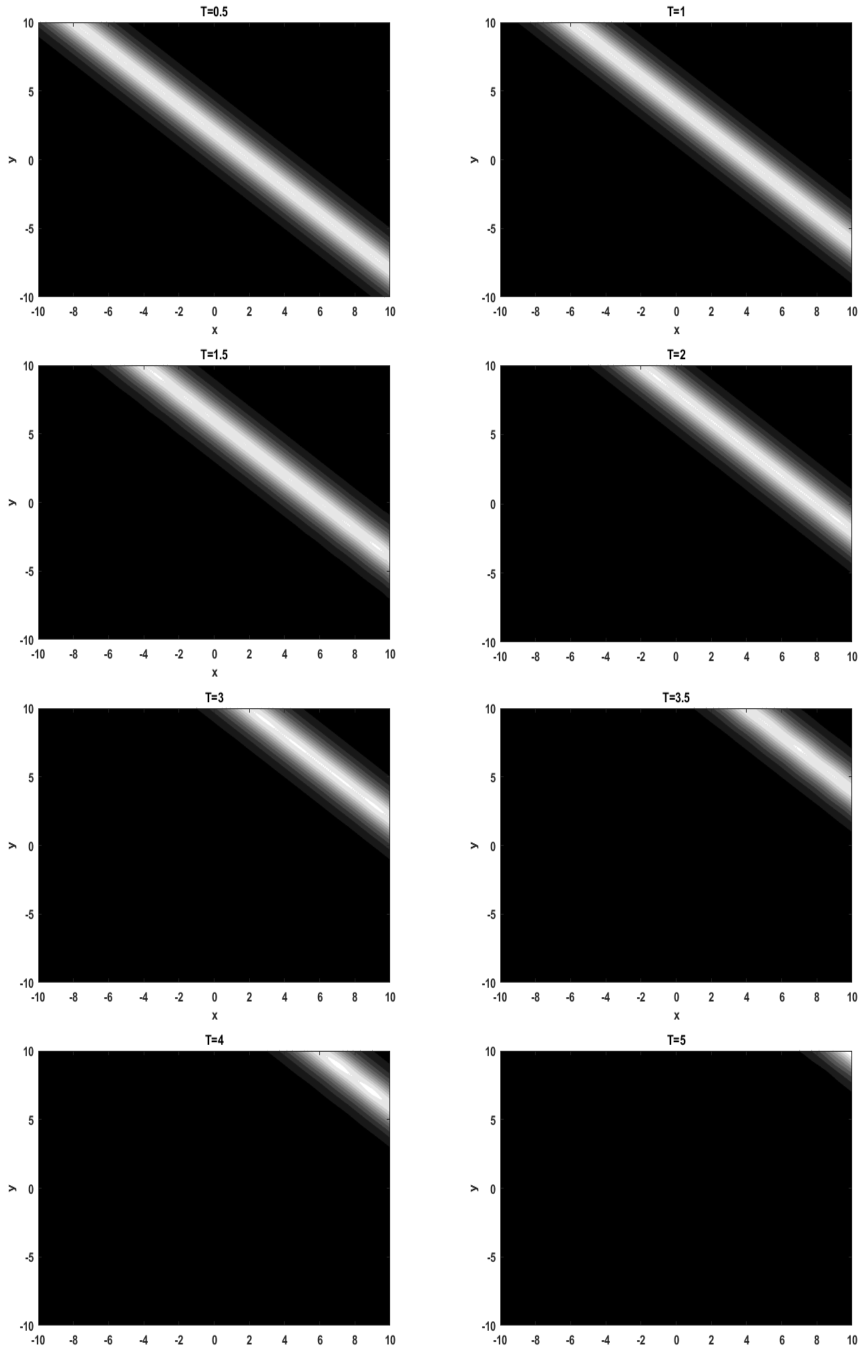

FIGURE 4. Approximation solution with its contour and graph of absolute error at final time $T = 1$ for Test problem 3.

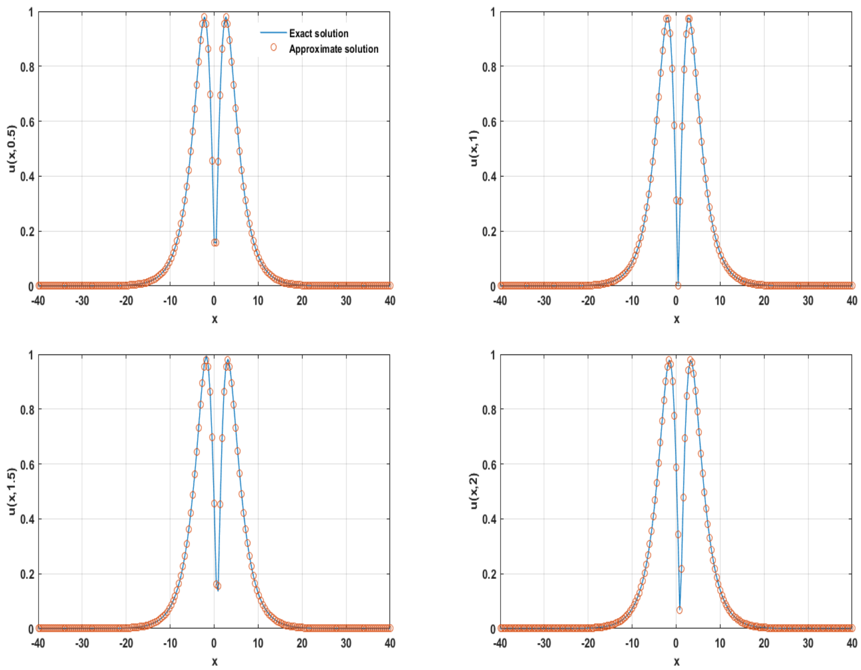

TABLE 7. Numerical results and computational orders with $h = 1/300$ for Test problem 4

τ	u L_∞	u C-order	v L_∞	v C-order
$\frac{1}{10}$	6.8257×10^{-1}	–	7.6431×10^{-1}	–
$\frac{1}{20}$	5.5556×10^{-2}	3.6189	6.3469×10^{-2}	3.5900
$\frac{1}{40}$	4.0679×10^{-3}	3.7716	4.6731×10^{-3}	3.7636
$\frac{1}{80}$	3.2279×10^{-4}	3.6556	3.6380×10^{-4}	3.6832
$\frac{1}{160}$	3.4238×10^{-5}	3.2369	3.6745×10^{-5}	3.3075
$\frac{1}{320}$	4.2010×10^{-6}	3.0268	4.3268×10^{-6}	3.0862
$\frac{1}{640}$	3.4658×10^{-7}	3.5994	3.4785×10^{-7}	3.6367

Table 8. Comparison between obtained errors for Test problem 4

h	Method of [28]	Method of [29]	Present method
1	8.5741×10^{-4}	9.5384×10^{-3}	2.4108×10^{-3}
1/2	2.8660×10^{-8}	4.8946×10^{-4}	3.3516×10^{-4}
1/4	1.6693×10^{-9}	3.2353×10^{-5}	2.9108×10^{-5}

Figure 5. Approximation solution with its contour and graph of absolute error at final time $T = 1$ for Test problem 5.

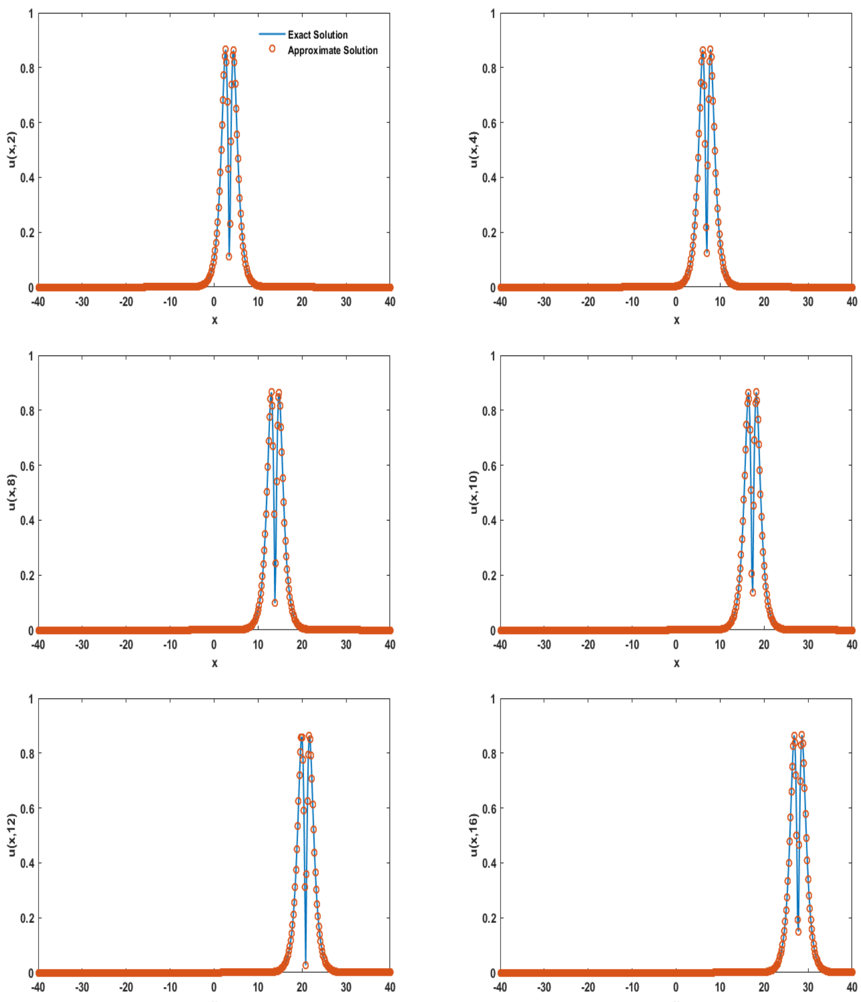

FIGURE 6. Approximation solution for Test problem 5.

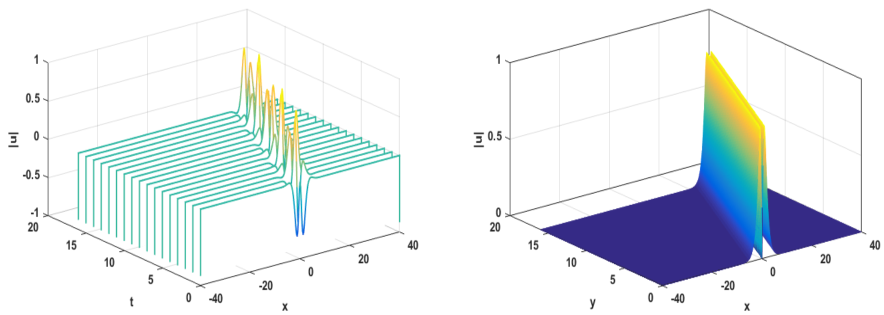

5.5. **Test problem 5.** We consider the Schrödinger-Boussinesq system as [28]

$$\begin{cases} i\dfrac{\partial u}{\partial t} + \gamma u_{xx} = \xi uv, \qquad x \in \Omega, \quad t > 0, \\ \dfrac{\partial^2 v}{\partial t^2} = v_{xx} - \alpha v_{xxxx} + (f(v))_{xx} + \omega(|u|^2)_{xx}, \qquad x \in \Omega, \quad t > 0, \end{cases} \tag{5.10}$$

with exact solution

$$\begin{cases} u(x,t) = \sqrt{\dfrac{18 b_1 d_1}{\omega \xi}}\, \mathrm{sech}(\mu\zeta) \tanh(\mu\zeta) e^{i\left(\frac{M}{2\gamma}x + \delta t\right)}, \\ v(x,t) = -\dfrac{6b_1}{\xi} \sec h^2(\mu\zeta), \end{cases} \tag{5.11}$$

in which

$$b_1 = \delta + \frac{M^2}{4\gamma}, \qquad d_1 = 1 - M^2, \qquad \mu = \sqrt{\frac{b_1}{\gamma}},$$

$$\zeta = x - Mt, \qquad \gamma = 1, \qquad \xi = -6, \qquad \alpha = 1,$$

$$\theta = 0, \qquad \omega = 2, \qquad M = \sqrt{3}, \qquad \delta = \frac{1}{4}.$$

We solve this equation using the proposed technique. Table 9 presents the error obtained to show the accuracy and computational order of time-discrete scheme with $h = 1/300$ for Test problem 4.

5.6. **Test problem 6.** (***Collision of triple solitons:***) In order to show the interactions of three solitons, we solve the system (1.4) with the following initial conditions

Table 9. Numerical results and computational orders for Test problem 5

	u		u	
τ	$h = 1/500$	C-order	$h = 1/400$	C-order
$\frac{1}{10}$	1.0342×10^{-1}	–	4.1999×10^{-1}	–
$\frac{1}{20}$	6.3888×10^{-3}	4.0168	2.5267×10^{-2}	4.0545
$\frac{1}{40}$	4.1282×10^{-4}	3.9520	2.0463×10^{-3}	3.6267
$\frac{1}{80}$	2.3636×10^{-5}	4.1264	6.2621×10^{-5}	5.0302
$\frac{1}{160}$	1.4721×10^{-6}	4.0050	3.7809×10^{-6}	4.0498
$\frac{1}{320}$	8.9649×10^{-9}	4.0374	2.3073×10^{-7}	4.0344

Figure 7. Graphs of three solitons interaction at different time t using the present method and with $h = 1/2$, $\tau = 40/40000$ and $c = 0.43$ on $[-20, 60]$ for Test problem 6.

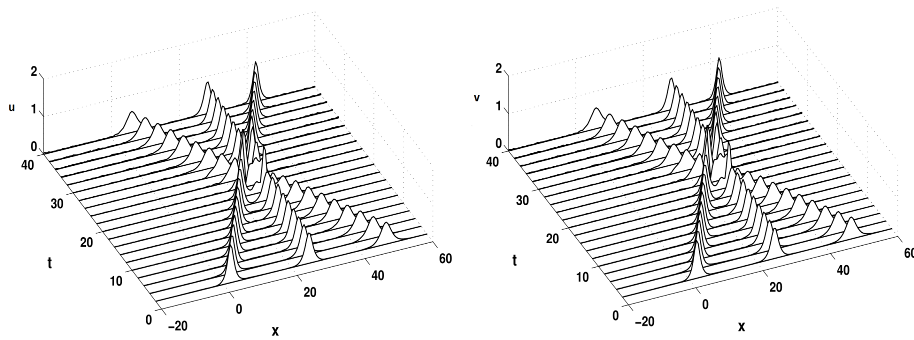

$$
\begin{cases}
u(x,0) = \displaystyle\sum_{j=1}^{3} \sqrt{\frac{2\alpha_j}{1+\beta}} \sec h\left(\sqrt{2\alpha_j} x_j\right) \exp\left(i v_j x_j\right), \\
v(x,0) = \displaystyle\sum_{j=1}^{3} \sqrt{\frac{2\alpha_j}{1+\beta}} \sec h\left(\sqrt{2\alpha_j} x_j\right) \exp\left(i v_j x_j\right),
\end{cases}
\tag{5.12}
$$

in which $x_1 = x$, $x_2 = x - 25$ and $x_3 = x - 50$. Also, we put $v_1 = 1$, $v_2 = 0$, $v_3 = -1$, $\alpha_1 = 1$, $\alpha_2 = 0.6$, $\alpha_3 = 0.3$, and $a(t) = b(t) = c(t) = h(t) = 1$.

Figure 7 presents the graphs of three solitons interaction at different time t using the present method with $h = 1/2$, $\tau = 40/40000$ and $c = 0.43$ on $[-20, 60]$ for Test problem 6. Figure 7 shows the time evolution of the three-soliton interactions at different times.

6. Conclusion

In this paper, we solved the generalized variable coefficient Schrödinger equation and Schrödinger-Boussinesq system using the smooth particle hydrodynamic (SPH) procedure. The SPH method is one of the meshless methods based on the strong form. At first, the spatial direction has been discretized based on the SPH technique and then a semi-discrete scheme is derived. The obtained semi-discrete scheme depends on time variable and also it is a system of ODEs. To get a high-order accurate numerical technique, we applied the fourth-order exponential time differenceing Runge-Kutta method (ETDRK4) for the obtained system of ODEs. Numerical results showed that the computational orders of time discrete are close to the theoretical convergence orders and confirm the efficiency of new method developed in the current paper.

Acknowledgment

The authors are grateful to the reviewers for carefully reading this paper and for their comments and suggestions which have improved the paper.

References

[1] D. Bai and J. Wang, *The time-splitting Fourier spectral method for the coupled Schrödinger–Boussinesq equations*, Communications in Nonlinear Science and Numerical Simulation, *17*(3) (2012), 1201–1210.

[2] D. Bai and L. Zhang, *The quadratic B-spline finite-element method for the coupled Schrödinger–Boussinesq equations*, International Journal of Computer Mathematics, *88*(8) (2011), 1714–1729.

[3] S. Bilige, T. Chaolu, and X. Wang, Application of the extended simplest equation method to the coupled Schrödinger–Boussinesq equation, Applied Mathematics and Computation, *224* (2013), 517–523.

[4] A. Bratsos, *A linearized finite-difference scheme for the numerical solution of the nonlinear cubic Schrödinger equation*, Journal of Applied Mathematics and Computing, *8*(3) (2001), 459–467.

[5] J. Chen and J. Beraun, *A generalized smoothed particle hydrodynamics method for nonlinear dynamic problems*, Computer Methods in Applied Mechanics and Engineering, *190*(1) (2000), 225–239.

[6] S. M. Cox and P. C. Matthews, *Exponential time differencing for stiff systems*, Journal of Computational Physics, *176*(2) (2002), 430–455.

[7] M. Dehghan and A. Shokri, *A numerical method for two-dimensional Schrödinger equation using collocation and radial basis functions*, Computers & Mathematics with Applications, *54*(1) (2007), 136-146.

[8] M. Dehghan and A. Taleei, *A compact split-step finite difference method for solving the nonlinear Schrödinger equations with constant and variable coefficients*, Computer Physics Communications, *181*(1) (2010), 43–51.

[9] M. Dehghan and R. Salehi, *A meshless based numerical technique for traveling solitary wave solution of Boussinesq equation*, Applied Mathematical Modelling, *36*(5) (2012), 1939–1956.

[10] M. Dehghan and V. Mohammadi, *Two numerical meshless techniques based on radial basis functions (RBFs) and the method of generalized moving least squares (GMLS) for*

simulation of coupled Klein-Gordon-Schrödinger (KGS) equations, Computers & Mathematics with Applications, *71*(4) (2016), 892–921.

[11] L. G. Farah and A. Pastor, On the periodic Schrödinger–Boussinesq system, Journal of Mathematical Analysis and Applications, *368*(1) (2010), 330–349.

[12] R. A. Gingold and J. J. Monaghan, *Smoothed particle hydrodynamics: theory and application to non-spherical stars*, Monthly Notices of the Royal Astronomical Society, *181*(3) (1977), 375–389.

[13] C. A. Gomez, A. H. Salas, and B. A. Frias, *New periodic and soliton solutions for the generalized BBM and Burgers–BBM equations*, Applied Mathematics and Computation, *217* (4) (2010), 1430–1434.

[14] B. Guo, *The global solution of the system of equations for complex Schrödinger field coupled with Boussinesq type self-consistent field*, Acta Math. Sinica, *26* (1983), 297–306.

[15] B. Guo and X. Du, *The behavior of attractors for damped Schrödinger-Boussinesq equation*, Communications in Nonlinear Science and Numerical Simulation, *6*(1) (2001), 54–60.

[16] B.-L. Guo and C. Feng-Xin, *Finite-dimensional behavior of global attractors for weakly damped and forced KDV equations coupling with nonlinear Schrödinger equations*, Nonlinear Analysis: Theory, Methods & Applications, *29*(5) (1997), 569–584.

[17] D. He and K. Pan, *An unconditionally stable linearized CCD-ADI method for generalized nonlinear Schrödinger equations with variable coefficients in two and three dimensions*, Computers & Mathematics with Applications, *73* (2017), 2360–2374.

[18] Y. Hon and E. Fan, *A series of exact solutions for coupled higgs field equation and coupled Schrödinger–Boussinesq equation*, Nonlinear Analysis: Theory, Methods & Applications, *71*(7) (2009), 3501–3508.

[19] A.-K. Kassam and L. N. Trefethen, *Fourth-order time-stepping for stiff PDEs*, SIAM Journal on Scientific Computing, *26*(4) (2005) 1214–1233.

[20] A. Khaliq, J. Martin-Vaquero, B. Wade, and M. Yousuf, *Smoothing schemes for reaction-diffusion systems with nonsmooth data*, Journal of Computational and Applied Mathematics, *223*(1) (2009), 374–386.

[21] A. Kılıcman and R. Abazari, *Travelling wave solutions of the Schrödinger-Boussinesq system*, in: Abstract and Applied Analysis, vol. 2012, Hindawi Publishing Corporation, 2012.

[22] H. Lang-Yang, J. Yan-Dong, and L. De-Min, *Multi-symplectic scheme for the coupled Schrödinger-Boussinesq equations*, Chinese Physics B, *22*(7) (2013), Article ID 070201.

[23] L. Z. Li, H.-W. Sun, and S.-C. Tam, *A spatial sixth-order alternating direction implicit method for two-dimensional cubic nonlinear Schrödinger equations*, Computer Physics Communications, *187* (2015), 38–48.

[24] X. Li, L. Zhang, and S. Wang, *A compact finite difference scheme for the nonlinear Schrödinger equation with wave operator*, Applied Mathematics and Computation, *219*(6) (2012), 3187–3197.

[25] Y. Li and Q. Chen, *Finite dimensional global attractor for dissipative Schrödinger–Boussinesq equations*, Journal of Mathematical Analysis and Applications, *205*(1) (1997), 107–132.

[26] X. Liang, A. Q. Khaliq, and Y. Xing, *Fourth order exponential time differencing method with local discontinuous Galerkin approximation for coupled nonlinear Schrödinger equations*, Communications in Computational Physics, *17*(02) (2015), 510–541.

[27] F. Liao and L. Zhang, *Conservative compact finite difference scheme for the coupled Schrödinger–Boussinesq equation*, Numerical Methods for Partial Differential Equations, *32*(6) (2016), 1667–1688.

[28] F. Liao, L. Zhang, and S. Wang, *Time-splitting combined with exponential wave integrator Fourier pseudospectral method for Schrödinger–Boussinesq system*, Communications in Nonlinear Science and Numerical Simulation, *55* (2018), 93–104.

[29] F. Liao and L. M. Zhang, *Conservative compact finite difference scheme for the coupled Schrodinger-Boussinesq equation*, Numer Methods Part Differ Eq, *32* (2016), 1667–1688.

[30] G. Liu, K. Dai, and T. Nguyen, *A smoothed finite element method for mechanics problems*, Computational Mechanics, *39*(6) (2007), 859–877.

[31] G.-R. Liu and M. B. Liu, *Smoothed Particle Hydrodynamics: a meshfree particle method*, World Scientific, 2003.

[32] M. R. Liu and G. R. Liu, *Smoothed particle hydrodynamics (SPH): an overview and recent developments*, Archives of Computational Methods in Engineering, *17*(1) (2010), 25–76.

[33] L. B. Lucy, *A numerical approach to the testing of the fission hypothesis*, The astronomical journal, *82* (1977), 1013–1024.

[34] M. A. Noor, K. I. Noor, A. Waheed, and E. A. Al-Said, *Some new solitonary solutions of the modified Benjamin–Bona–Mahony equation*, Computers & Mathematics with Applications, *62*(4) (2011), 2126–2131.

[35] G. Oger, D. Le Touzé, D. Guibert, M. De Leffe, J. Biddiscombe, J. Soumagne, and J.-G. Piccinali, *On distributed memory MPIi-based parallelization of SPH codes in massive HPC context*, Computer Physics Communications, *200* (2016), 1–14.

[36] N. N. Rao, *Exact solutions of coupled scalar field equations*, Journal of Physics A: Mathematical and General, *22* (1989), 4813–4825.

[37] J. Ren, T. Jiang, W. Lu, and G. Li, *An improved parallel SPH approach to solve 3D transient generalized Newtonian free surface flows*, Computer Physics Communications, *205* (2016), 87–105.

[38] Y. Ruoxia and L. Zhibin, *Exact explicit solutions of the nonlinear Schrödinger equation coupled to the Boussinesq equation*, Acta Mathematica Scientia, *23* (4) (2003), 453–460.

[39] A. Shokri and M. Dehghan, *A Not-a-Knot meshless method using radial basis functions and predictor-corrector scheme to the numerical solution of improved Boussinesq equation*, Computer Physics Communications, *181*(12) (2010), 1990-2000.

[40] A. Taleei and M. Dehghan, *Time-splitting pseudo-spectral domain decomposition method for the soliton solutions of the one-and multi-dimensional nonlinear Schrodinger equations*, Computer Physics Communications, *185*(6) (2014), 1515-1528.

[41] S. Wang and L. Zhang, *Split-step orthogonal spline collocation methods for nonlinear Schrödinger equations in one, two, and three dimensions*, Applied Mathematics and Computation, *218*(5) (2011), 1903–1916.

[42] T. Wang, B. Guo, and Q. Xu, *Fourth-order compact and energy conservative difference schemes for the nonlinear Schrödinger equation in two dimensions*, Journal of Computational Physics, *243* (2013), 382–399.

[43] A. M. Wazwaz, *Reliable analysis for nonlinear Schrödinger equations with a cubic nonlinearity and a power law nonlinearity*, Mathematical and Computer Modelling, *43* (2006), 178–184.

[44] A. M. Wazwaz, *Exact solutions for the fourth order nonlinear Schrödinger equations with cubic and power law nonlinearities*, Mathematical and Computer Modelling, *43* (2006), 802–808.

[45] Z. Wei and R. A Dalrymple, *SPH modeling of short-crested waves*, arXiv preprint arXiv:1705.08547, 2017.

[46] Z. Wei, R. A. Dalrymple, A. Herault, G. Bilotta, E. Rustico, and H. Yeh, *SPH modeling of dynamic impact of tsunami bore on bridge piers*, Coastal Engineering, *104* (2015), 26–42.

[47] Z. Wei and R. A. Dalrymple, *Numerical study on mitigating tsunami force on bridges by an SPH model*, Journal of Ocean Engineering and Marine Energy, *2* (2016), 365–380.

[48] Z. Wei, R. A. Dalrymple, E. Rustico, A. Herault, and G. Bilotta, *Simulation of nearshore tsunami breaking by smoothed particle hydrodynamics method*, Journal of Waterway, Port, Coastal and Ocean Engineering, *142*(4) (2016), 05016001.

[49] Z. Wei and R. A Dalrymple, *SPH modeling of vorticity generation by short-crested wave breaking*, Coastal Engineering Proceedings, *35* (2016), 1–12.

[50] D. Winkler, M. Meister, M. Rezavand, and W. Rauch, *gpuSPHASE-A shared memory caching implementation for 2D SPH using CUDA*, Computer Physics Communications, *213* (2017), 165–180.

[51] X. Xu and X.-L. Deng, *An improved weakly compressible sph method for simulating free surface flows of viscous and viscoelastic fluids*, Computer Physics Communications, *201* (2016), 43–62.

[52] Y. Xu and L. Zhang, *Alternating direction implicit method for solving two-dimensional cubic nonlinear Schrödinger equation*, Computer Physics Communications, *183*(5) (2012), 1082–1093.

[53] N. Yajima and J. Satsuma, *Soliton solutions in a diatomic lattice system*, Progress of Theoretical Physics, *62*(2) (1979), 370–378.

[54] C. Zhang, X. Hu, and N. Adams, *A weakly compressible SPH method based on a low-dissipation Riemann solver*, Journal of Computational Physics, *335* (2017), 605–620.

[55] L. Zhang, D. Bai, and S. Wang, *Numerical analysis for a conservative difference scheme to solve the Schrödinger–Boussinesq equation*, Journal of Computational and Applied Mathematics, *235*(17) (2011), 4899–4915.